ACS Catalysis

RESEARCH ARTICLE

pubs.acs.org/acscatalysis

Surface Impregnation Combustion Method to Prepare Nanostructured Metallic Catalysts without Further Reduction: As-Burnt Co/SiO_2 Catalysts for Fischer−Tropsch Synthesis

Lei Shi,[†] Kai Tao,[†] Tokimasa Kawabata,[†] Takeshi Shimamura,[†] Xue Jun Zhang,[‡] and Noritatsu Tsubaki*[,†]

[†]Department of Applied Chemistry, School of Engineering, University of Toyama, Gofuku 3190, Toyama, 930-8555, Japan

[‡]Department of Applied Chemistry, Shenyang University of Chemical Technology, Shenyang 110142, P.R. China

Supporting Information

ABSTRACT: A series of the as-burnt supported metallic catalysts (Co/SiO_2) were prepared by a novel surface impregnation combustion method using cobalt nitrates (noted as M) and citric acid (noted as CA), and burnt in the argon atmosphere. H_2 and CH_4 which were derived from the decomposition of the CA, acted as the reducing agents for synthesizing metallic Co from Co^{2+} in the chelated compounds. The X-ray diffraction (XRD) patterns revealed that all the as-burnt catalysts with different M/CA molar ratios were converted into Co and CoO species supported on SiO_2 (Q-50). The as-burnt catalyst $C_{1.5}$, with M/CA = 1/1.5, was almost fully converted to metallic Co species and amorphous carbon supported on SiO_2. With increase of the content of CA in the initial precursors, the reduction degree of the as-burnt catalysts which was measured by temperature-programmed reduction (TPR) and the dispersion of metallic cobalt increased gradually. The as-burnt catalysts were used directly in slurry-phase Fischer-Tropsch synthesis (FTS) without further reduction. The effects of M/CA molar ratios on the properties of the as-burnt catalysts were studied by TG-DTA measurement in the argon atmosphere, XRD, FT-IR, Raman spectrum, TPR, H_2-chemisorption, and transmission electron microscopy (TEM). The amount of amorphous carbon left in the as-burnt catalysts was measured by energy dispersive spectroscopy (EDS) analysis and TG-DTA measurement in air. Comparing with the Co/SiO_2 catalyst prepared by the conventional impregnation method (noted as C_N) which was followed by 10 h reduction at 723 K in hydrogen, the CO conversion of the as-burnt Co/SiO_2 catalyst (without reduction) with M/CA = 1/1 was almost 3-fold of that of the catalyst C_N. This surface impregnation autocombustion method may open a new way to prepare metallic catalysts without further reduction, especially the catalysts which were difficult to be reduced at higher temperature.

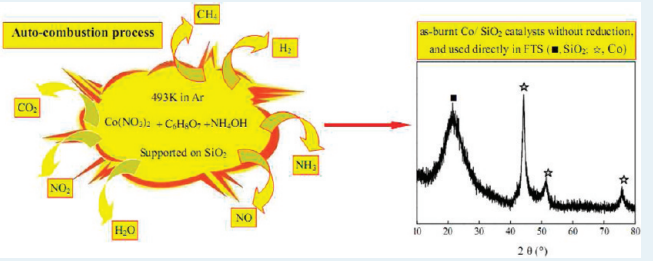

KEYWORDS: metallic catalysts, reduction-free, autocombustion, surface impregnation, Co/SiO_2, Fischer−Tropsch synthesis

1. INTRODUCTION

Supported metallic catalysts have been widely used in catalytic reactions, as a function of hydrogenation, dehydrogenation, isomerization,[1] reforming, selective hydrocarbon oxidation,[2] and so on. Recently, nanostructured metallic catalysts[3−5] received widespread interest because of a large concentration of surface active sites. For Fischer−Tropsch synthesis (FTS), the catalytic performance of cobalt based catalysts was strongly affected by the size of cobalt metal particles.[6−12] Conventional cobalt FT catalysts[6−14] were prepared by aqueous impregnation of supports with solutions of cobalt nitrates and followed by drying. After decomposition of the supported cobalt nitrates by calcination in the air atmosphere, the catalysts were reduced in pure hydrogen at higher temperature to generate metallic cobalt sites. However, Co crystalline size prepared from nitrates by these methods became as large as more than 20 nm. Chu et al. used glow-discharge nitrogen plasma and hydrogen plasma to pretreat cobalt catalyst, and then the catalysts were reduced in pure hydrogen at 673 K for 5 h to obtain a cobalt crystalline size of about 10 nm.[15] De Jong et al. decomposed cobalt or nickel nitrates in an NO/He atmosphere to obtain supported NiO and Co_3O_4 particles with a diameter of 4−5 nm, and then the cobalt catalyst was reduced by H_2/He at 823 K for 5 h.[16]

Here, we present a novel surface impregnation autocombustion method to obtain uniform and nanostructured (Co size: 4−6 nm) Co/SiO_2 catalysts without further reduction and used directly in slurry phase Ficher-Tropsch synthesis. This technique was based on a chemical sol−gel process combined with a subsequent combustion process.[17] An aqueous solution containing the desired metal salts and organic fuel impregnated on the support, forming the xerogel through the sol−gel process, and then the xerogel was ignited to combust in the argon atmosphere, giving a voluminous and fluffy product with a large surface area. In this process, citric acid (noted as CA) was generally used as reductant and a kind of chelated agent providing complexing

Received: June 4, 2011
Revised: August 9, 2011
Published: August 15, 2011

ligands, forming a homogeneous precursor. The main advantage of this novel surface impregnation autocombustion method is that nanostructured metallic catalysts, including basic metallic catalysts and noble metallic catalysts, can be prepared directly without further reduction. This surface impregnation autocombustion method may open a new way to prepare metallic catalysts without further reduction, especially the catalysts which were difficult to be reduced at higher temperature.

2. EXPERIMENTAL SECTION

2.1. Catalyst Preparation. The catalyst was prepared by wetness impregnation on a commercially available silica gel (Cariact Q-50, Fuji Silysia Co., specific surface area: 57 $m^2\ g^{-1}$, pore volume: 1.2 mL g^{-1}). Analytical-grade $Co(NO_3)_2 \cdot 6H_2O$ (≥99%) and CA were used as raw materials. The cobalt nitrates (noted as M) and CA were first dissolved in 150 mL of distilled water according to different M/CA molar ratios of 1:0.5, 1:07, 1:1, and 1:1.5, denoted as $C_{0.5}$, $C_{0.7}$, C_1, and $C_{1.5}$, respectively. The solutions were adjusted using ammonia of 28% (wt %) to reach a pH value of 7. Stirring and refluxing at 353 K for 4 h ensured the CA completely chelated with the metal ions. Subsequently, the neutralized solution was evaporated at 343 K on a hot plate with continuous stirring, until 6 mL (the concentration about 2.5 mol/L Co^{2+}) of a dark red solution was left. The catalysts with 15 wt % cobalt metal loading were prepared by wetness impregnation of 5 g of silica (Q-50), with the as-prepared 6 mL of the dark red cobalt aqueous solution. The obtained catalyst precursors were dried in air at 393 K for 12 h, then calcined in argon from room temperature to 723 K with a ramping rate of 2 K min^{-1} and kept at 723 K for 3 h, subsequently passivated by 1% oxygen in the argon at room temperature for 4 h, then the as-burnt catalysts were directly used for FT synthesis without H_2 reduction. For comparison, Cobalt supported catalyst with 15 wt % metal loading was prepared by the incipient-wetness impregnation method on Q-50 (noted as C_N) which was reduced at 723 K for 10 h in pure hydrogen, as described elsewhere.[10]

2.2. Ficher-Tropsch Synthesis Reaction. The reaction performance of the catalysts in FTS was carried out in a semibatch slurry-phase reactor with an inner volume of 80 mL. Passivated catalyst of 1.0 g was loaded in the reactor with 20 mL of *n*-hexadecane as liquid medium. The reaction conditions were P (total) = 1.0 MPa, T = 513 K, CO/H_2 = 1/2, W/F (CO + H_2 + Ar) = 10 g h mol^{-1}. The effluent gas from the reactor was analyzed by online gas chromatography. A thermal conductivity detector (TCD) was used to analyze gaseous products (CO, CO_2, and CH_4). 3% Ar was used as inner standard. Light hydrocarbons (C_1−C_5) were online analyzed by a flame ionization detector (FID) with a Porapak-Q column. The analysis of hydrocarbons dissolved in the solvent and cooled in the trap was carried out by FID with a silicone SE-30 column.

2.3. Characterization of Catalysts. The thermal decomposition behavior of the xerogels was characterized by thermogravimetic and differential thermal analysis (DTA/TGA 60, Shimadzu) at a heating rate 10 K min^{-1} from 293 to 973 K in the argon atmosphere. The content of amorphous carbon left in the as-burnt catalysts was also measured by DTA/TGA 60 at a heating rate 10 K min^{-1} from 293 to 1073 K in the air atmosphere.

Xray diffraction (XRD) patterns were obtained on a Rigaku RINT 2400 X-ray diffractometer in the air, using monochromatic Cu Kα radiation, scanning 2 θ from 20 to 80°, and at 40 kV and 40 mA. The cobalt crystalline average size was calculated by the Scherrer formula $D = K\lambda/(\beta \cos \theta)$.

Infrared spectra were recorded in the air with a Shimadzu Fourier Transform Infrared Spectrophotometer (FTIR-8400).

Micro-Raman analysis of specimens was performed on a multichannel bench Renishaw InVia Reflex spectrometer coupled with a Peltier-cooled CCD detector. The instrument was equipped with a 514 nm diode laser for excitation, with a maximum output power of 100 mW. The samples were scanned from 800 to 2400 cm^{-1} because this spectrum region provided the most valuable data on the microstructure of carbon and carbonates.

The physical structures of the catalysts, as well as compositional analysis and surface morphology observation, were measured by scanning electron microscopy (SEM) (JEOL, JSM-6360 LV) with energy-diffusive X-ray spectroscopy (EDX) (JEOL, JED-2300). The samples for this analysis were first coated with a platinum layer on the surface by an auto fine coater (JEOL, JFC-1600).

The reduction behavior and the reduction degree of the supported metal oxide phases were studied by hydrogen temperature-programmed reduction (H_2-TPR) using the catalyst analyzer BELCAT-B, using 0.025 g of calcined catalysts with 5% hydrogen diluted by argon at atmospheric pressure. Before reduction, the catalysts were heated at 323 K in flowing argon for 2 h. Then, the 5% hydrogen (50 mL/min) was passed over the catalyst sample, and the temperature was linearly raised from 298 to 1023 K at a heating rate of 5.0 K/min. Water, formed during the reduction, was trapped by molecular sieves 3A. The effluent gas was analyzed by a thermal conductivity detector (TCD), with argon as a reference. The reduction of CuO was used to calibrate the TCD signal for H_2 consumption.[18,19] The reduction degree corresponding to the TPR curves was calculated from the area of the peaks assuming Co_3O_4 as a main component to be reduced.

Transmission electron microscopy (TEM) images were obtained by TOPCON EM-002 B operated at 200 kV. A catalyst pellet was embedded into resin and cut by the microtome method (Leica Ultracut UCT). The observation was implemented on JEOL TEM-2010. Average particle size was estimated according to $\Sigma n_i d_i^3/\Sigma\Sigma n_i d_i^2$.

The active metal surface of the catalyst was measured by H_2-chemisorption experiments which were carried out in a static volumetric glass high-vacuum system (Quantacharome Autosorb-1). The chemisorbed H_2 was measured at 373 K using the double-isotherms method as described by Bartholomew et al.[20,21] Bartholomew et al. reported that H_2 chemisorption at 373 K was most reliable for silica-supported cobalt catalysts. Prior to adsorption, the catalysts C_N after reduction and the as-burnt catalysts without reduction (0.2−0.5 g) were pretreated in flowing He at 393 K for 1 h. Afterward, the temperature was raised from 393 to 723 K at a heating rate of 1 K/min and maintaining this temperature for 5 h. Thereafter, the catalysts were degassed at 1.3 Pa, and the temperature lowered to 373 K. Average crystallite diameters in nanometers were calculated from D% assuming spherical metal crystallites of uniform diameter d with a site density of 14.6 at/nm^2. Thus, d = 96/D, where D% was the percentage dispersion.

3. RESULTS AND DISCUSSION

3.1. TG-DTA Analysis of CA and the Precursors of the As-Burnt Catalysts with Different M/CA Molar Ratios to Study the Surface Impregnation Autocombustion Process. Thermal behavior of pure CA and the precursors of the as-burnt

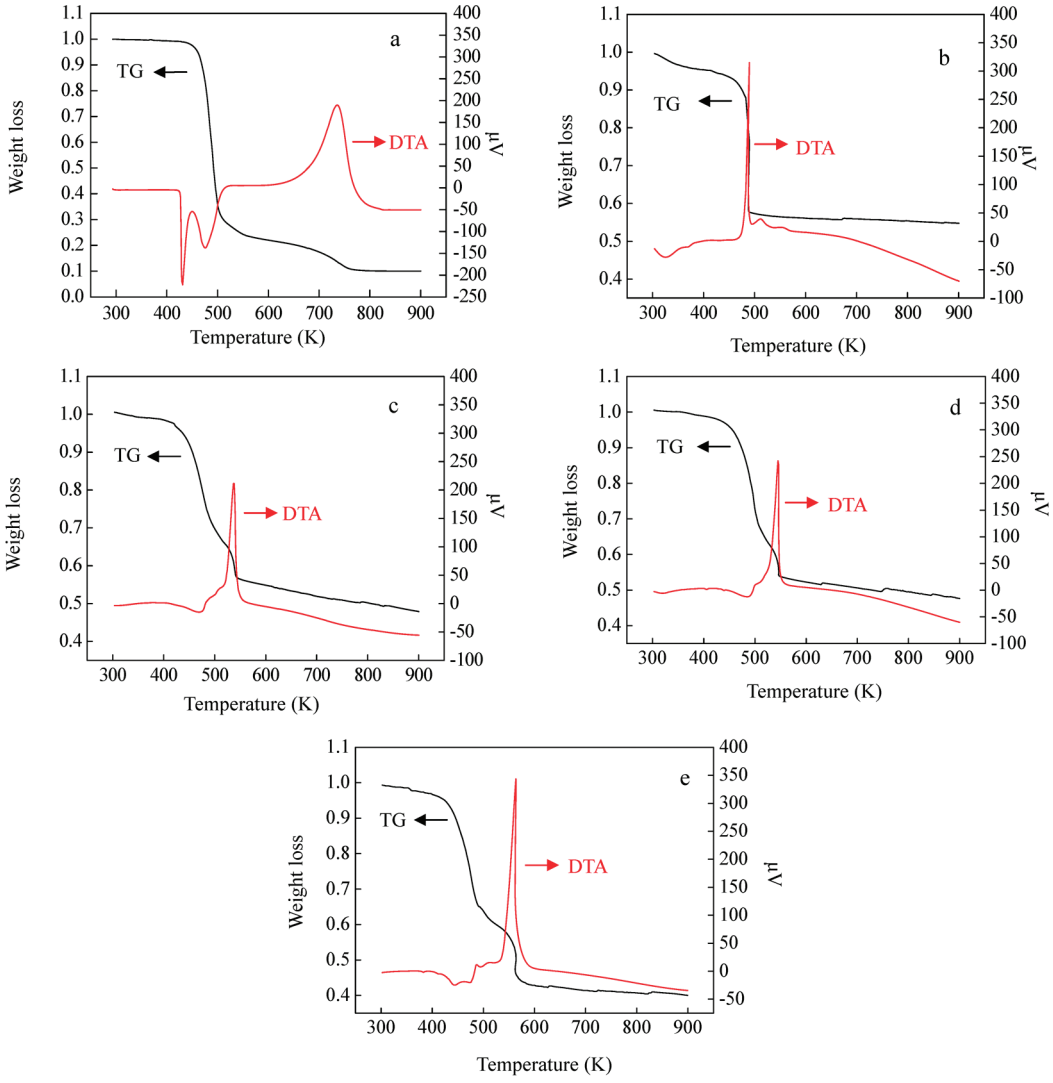

Figure 1. TG-DTA curves of (a) CA, as well as the precursors of the as-burnt catalysts with different M/CA molar ratios: (b) 1:0.5, (c) 1:0.7, (d) 1:1, and (e) 1:1.5.

catalysts with different M/CA molar ratios were investigated by TG-DTA measurements in the argon atmosphere. The results of the TG-DTA curves were compared in Figure 1. The DTA plots of pure CA (as compared in Figure 1a) presented two endothermic peaks at 440 and 483 K, and one exothermic peak at 743 K. The endothermic peak at 440 K could be assigned to the melting of the CA, and there was no weight loss. Another endothermic peak at 483 K came from the decomposition of CA,[17,22] releasing CH_4, H_2, H_2O, and CO_2, resulting in a large weight loss. The exothermic peak at 743 K arose from the pyrolysis of the residue organics at higher temperature. At last, about 10% weight of carbonic residues was left, as observed from the TG curve.

The DTA curve of Figure 1b presented only one sharp exothermic peak at about 493 K, and at the same time the TG curves showed an abrupt weight loss, which indicated that the combustion process of precursors happened as a severe redox reaction wherein CA acted as reductant and nitrate ions acted as oxidant. During this combustion process, a large amount of gases such as H_2, H_2O, CH_4, NO, CO_2, NH_3, NO_2 were liberated according to the literatures.[17,23] H_2 and CH_4 were the reducing agents that could be used in the redox process for obtaining metallic Co from Co^{2+} in the chelated compounds. The whole reduction process could be separated to four steps: (1) the decomposion of NH_4NO_3 at about 440 K; (2) generation of CH_4 and H_2 by the decomposition of CA at the beginning of 483 K; (3) redox process between CH_4-H_2 and NO_3^- at about 493 K; (4) reduction of metallic Co from Co^{2+} in the chelated compounds by CH_4 and H_2, with the heat from (3).

As well-known, the redox process was strongly influenced by the molar ratio of reductant to oxidant. Increase of the content of reductant made the redox process much gentler. As compared in Figure 1c−1e, there was only a small exothermic peak at about 493 K. It proved that the combustion process was smooth and the flame temperature of the combustion process was low. The second exothermic peaks between 530 and 580 K in Figure 1c−1e arose from the pyrolysis of the residue organics. Complicated carbonic residues left in the as-burnt catalysts were further proved by FT-IR, Raman spectrum, energy dispersive spectroscopy (EDS) analysis, and TG-DTA measurements in air. As compared in Figure 1c−1e, the area of the second exothermic peak in DTA curves and the weight loss of the precursors in TG curves increased with increase of the content of CA. It was

dx.doi.org/10.1021/cs200294d |ACS Catal. 2011, 1, 1225–1233

considered that more complicated carbonic residues which were derived from the pyrolysis of the residue organics were left in the as-burnt catalyst with increase of the content of CA.

It could be proved that H_2 and CH_4 were the reducing agents that could be used in the redox process for obtaining metallic Co, and the fierceness and the flame temperature of the combustion process were strongly influenced by the initial content of CA in the precursors. Decreasing the content of CA made the flame temperature higher, and the combustion process more severe, while continually increasing the content of the CA led to more carbonic residues left in the as-burnt catalysts.

3.2. XRD Analysis for the Calcined Catalyst C_N and the As-Burnt Catalysts with Different M/CA Molar Ratios. The XRD patterns of the reference catalyst which was prepared by the conventional incipient-wetness impregnation method and reduced in hydrogen at 723 K for 10 h (noted as C_N), and the as-burnt catalysts with different M/CA molar ratios were compared in Figure 2. All the diffraction peaks of C_N in Figure 2a were indexed to the Co^0 phase. But all the diffraction peaks of the as-burnt catalyst $C_{0.5}$ in Figure 2b were indexed to the CoO phase. There was almost no Co^0 phase. With increase of the initial content of CA in the precursors, Co species were gradually reduced from CoO phase to metallic Co^0. There was only Co^0 phase in Figure 2e ($C_{1.5}$), as the reduction degree of the as-burnt catalysts was strongly influenced by the content of reductant. H_2 and CH_4 were the reducing agents which came from the decomposition of the CA during the autocombustion process. By increasing the content of CA, more H_2 and CH_4 were liberated.

The crystalline size of the as-burnt catalysts with different M/CA molar ratios calculated by the Scherrer formula is presented in Table 1. For the as-burnt catalyst $C_{0.5}$ with M/CA = 1/0.5, the characteristic peaks were attributed to CoO phase only. So the cobalt particle size of $C_{0.5}$ was estimated by the crystalline size of CoO using the Scherrer equation. For the as-burnt catalyst $C_{0.7}$ and C_1, the characteristic peaks of CoO phase and Co at about 42−44° were overlapped. Here it was assumed that the characteristic peak's shape of metallic Co was symmetrical. On the basis of this assumption, the overlapped characteristic peaks were separated into independent CoO peak and Co peak, and the cobalt crystalline size was calculated by the Scherrer equation on the separated peak of Co. It was displayed that metallic Co particle size of C_N was about 28 nm. However, metallic Co particle sizes of the as-burnt catalysts were significantly smaller than that of C_N. It could be inferred that smaller Co crystalline size was obtained when using this novel surface impregnation autocombustion method. As compared in Figure 2 and Table 1, with increase of the content of CA, the Co crystalline size decreased gradually. The $C_O{}^0$ crystalline size of the as-burnt catalyst $C_{1.5}$ was only about 4 nm. It could be concluded that Co particle sizes were closely related to the M/CA molar ratio, which played an important role on the flame temperature in the autocombustion process. Decreasing the content of the CA made the flame temperature higher and the autocombustion process more severe. Higher temperature resulted in the larger Co particle size. These findings were in accordance with the combustion fierceness degree which was illustrated by the TG-DTA curves in Figure 1.

3.3. FT-IR Analysis of SiO_2-Free Precursors and the As-Burnt Catalysts with Different M/CA Molar Ratios. The FT-IR spectrum of the SiO_2-free precursors with different M/CA molar ratios was compared in Figure 3. A broad absorption band at around 3180 cm^{-1} indicated the presence of adsorbed moisture.[24]

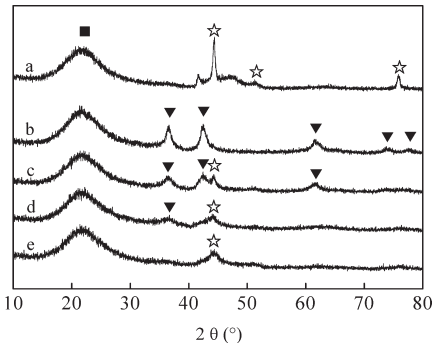

Figure 2. XRD patterns of (a) C_N as well as the as-burnt catalysts (b) $C_{0.5}$, (c) $C_{0.7}$, (d) C_1, and (e) $C_{1.5}$ (■, SiO_2; ☆, Co; ▼, CoO).

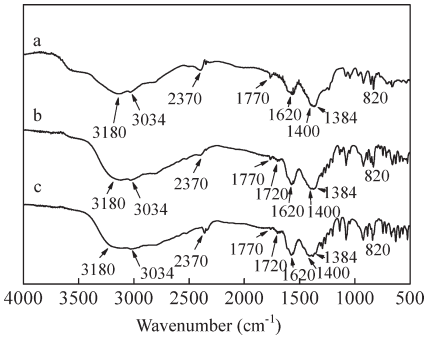

Figure 3. FT-IR spectrum of SiO_2-free precursors with different M/CA molar ratios of (a) 1:0.5, (b) 1:0.8, and (c) 1:1.5.

Table 1. Catalyst Characterization Results

	H_2 uptake[a]	reduction degree[b]	dispersion[c]	Co particle size (nm)		
catalysts	μmol H_2/g	TPR (%)	Co (%)	$H_{2(ad)}$[d]	XRD[e]	TEM
C_N[f]	32.3	82	3.1	31.0	28.4	30.0
$C_{0.5}$	n.d.[g]	32			8.5[h]	10.0
$C_{0.7}$	100.9	62	12.8	7.5	5.8	7.0
C_1	172.1	89	15.2	6.3	5.2	5.5
$C_{1.5}$	200.6	95	16.6	5.8	4.0	3.0

[a] H_2−Chemisorption without reduction, adsorption temperature was 373 K. [b] Calculated by TPR profiles. [c] Assuming the stoichiometry $H_{ad}/Co_s = 1$. [d] Calculated by 96/Dispersion. [e] Calculated by the Scherrer formula. [f] Reduced at 723 K for 10 h in hydrogen, then passivated by 1% O_2 in argon for 4 h. [g] n.d. = Not determined. [h] CoO Crystalline size.

dx.doi.org/10.1021/cs200294d |ACS Catal. 2011, 1, 1225–1233

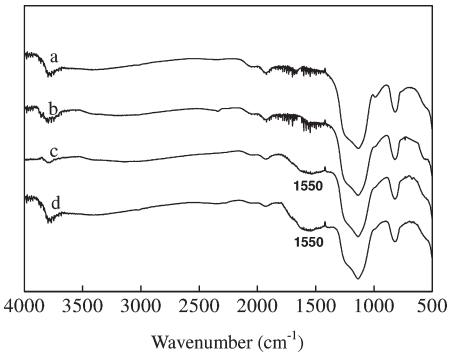

Figure 4. FT-IR spectrum of (a) SiO_2 as well as the as-burnt catalysts (b) $C_{0.5}$, (c) C_1, and (d) $C_{1.5}$.

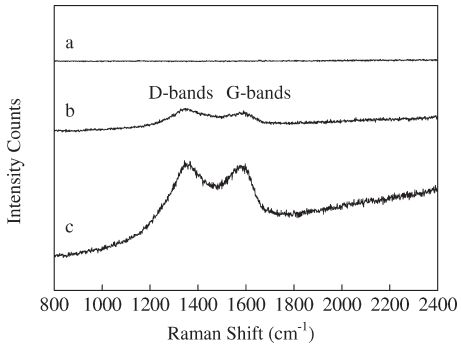

Figure 5. Raman analysis of the as-burnt catalysts (a) $C_{0.5}$, (b) C_1, and (c) $C_{1.5}$.

The band at 2370 cm^{-1} was attributed to the absorption of CO_2.[24,25] The bands at 820 and 1384 cm^{-1} were assigned to the NO_3^- and the band at 3034 $cm^{-1}$was assigned to O−H group.[24−26] Two bands occurred near 1620 and 1400 cm^{-1}, representing the asymmetric stretching and symmetric stretching vibrations for carboxyl ions (COO^-), while the bands at 1720 and 1770 cm^{-1} were from the free carboxylic group.[26,27] CA had two types of carboxyl groups, one inner carboxyl group (1770 cm^{-1}) and two terminal free carboxyl groups (1720 cm^{-1}). There were two bands at 1720 and 1770 cm^{-1} in Figure 3b and 3c, but no bands at 1720 cm^{-1} in Figure 3a, indicating that two terminal free carboxyl groups were completely chelated in the precursors with M/CA = 1/0.5.

Comparing with the FT-IR spectrum of SiO_2 in Figure 4a, there were almost no bands in Figure 4b. It implied that little carbonic residues left in the as-burnt catalyst $C_{0.5}$. Broad bands from about 1420 to 1750 cm^{-1} were presented in Figure 4c and 4d. The bands at 1428, 1534, 1551, and 1582 cm^{-1} were attributed to carbonates species (COOO),[28,29] and those at about 1650 cm^{-1} to C−O stretching vibration of bicarbonate.[29] It was clear that with increase of the initial content of CA in the precursors, the FT-IR bands (in the region from about 1420 to 1750 cm^{-1}) of the as-burnt catalyst increased gradually. It was inferred that more carbonic residues were left in the as-burnt catalysts with the increased content of CA.

3.4. Raman Analysis of the As-Burnt Catalysts with Different M/CA Molar Ratios. The Raman spectrum of the as-burnt catalysts was compared in Figure 5 in the region from 800 to 2400 cm^{-1}. There were no bands in Figure 5a. Two relatively broad Raman bands at about 1340 and 1590 cm^{-1}, which correspond to the D (disordered) and G (graphitic) bands of the amorphous carbon,[30,31] are exhibited in Figure 5b and 5c. With increase of the content of the CA, the band at about 1340 and 1590 cm^{-1} gradually increased. It was concluded that the amount of the amorphous carbon left on the surface of the as-burnt catalysts increased with increase of the content of CA.

3.5. SEM-EDS Analysis of the As-Burnt Catalysts. SEM micrographs and the EDS analysis of the as-displayed SEM micrographs of the as-burnt catalysts were compared in Figure 6. The crushed images of these three as-burnt catalysts were nearly the same. As exhibited in Figure 6a−6c, the area of carbon and cobalt element was not clear enough, so the weight ratio of the element which was measured by EDS analysis was added. It was compared in Figure 6a−6c; the weight ratio of cobalt element was about 15%, which was in accordance with the original experiment design. About 3.54% (weight ratio) carbon element stayed on the surface of the as-burnt catalyst $C_{0.5}$ in Figure 6a, about 9.43% carbon element left in the as-burnt catalyst C_1 in Figure 6b, and about 13.87% carbon element left in the as-burnt catalyst $C_{1.5}$ in Figure 6c. It was indicated that a part of carbonic residues left in the as-burnt catalysts, which was associated with the content of CA. Increasing the content of CA resulted in the increased content of carbonic residues, which were derived from the pyrolysis of the residue organics left on the surface, and the decreased content of O element. This trend implied that more carbonic residues were left on the surface of the as-burnt catalysts with increase of the initial content of CA in the precursors. These results were in accordance with the experimental phenomena that amorphous carbon which was proved by Raman spectrum, and carbonates species which were proved by FT-IR, were left in the as-burnt catalysts.

3.6. TG-DTA Analysis in the Air Atmosphere to Study the Content of Amorphous Carbon Left in the As-Burnt Catalysts. The content of amorphous carbon left in the as-burnt catalysts was investigated by TG-DTA measurements in air with a flow of 50 mL/min and at a heating rate of 10 K min^{-1} from 293 to 1073 K. The TG and DTA curves were offset by a few units to avoid the overlapping of the plots. Figure 7a1 and Figure 7b1 compared the TG and DTA curve of the catalyst C_N after 10 h reduction in pure hydrogen. It was shown that there was about 1.6% weight increase from about 430 to 510 K, and at the same time the DTA curve displayed a broad exothermic peak which was attributed to the oxidation of Co to Co_3O_4. As compared in Figure 7c1−7e1, there was also a little weight increase from about 430 to 510 K, and at the same time the DTA curves compared a small broad exothermic peak, suggesting that pure Co or CoO phase was in the as-burnt catalysts $C_{0.7}$, C_1, and $C_{1.5}$ without further reduction before oxidation by air. For the as-burnt catalyst $C_{0.5}$, there was no weight increase shown in Figure 7b1, but a small broad exothermic peak was also presented in figure b2, which indicated that some Co or CoO phase was still in the as-burnt catalysts $C_{0.5}$. These results were in accordance with the fact that the main composition of the as-burnt catalyst $C_{0.5}$ was CoO phase, not metallic Co, which was proved by XRD analysis. The weight increase from CoO to Co_3O_4 phase was limited and was easily counteracted by the release of adsorbed gases or moisture on the surface of the as-burnt catalyst $C_{0.5}$.

The main weight loss of the as-burnt catalysts (without reduction) from about 510 to 600 K arose from the amorphous carbon oxidation in the presence of cobalt, which was in accordance with the experimental results reported by Zhang et al.[32] and Schüth et al.[33] Amorphous carbon oxidation was a

dx.doi.org/10.1021/cs200294d |ACS Catal. 2011, 1, 1225–1233

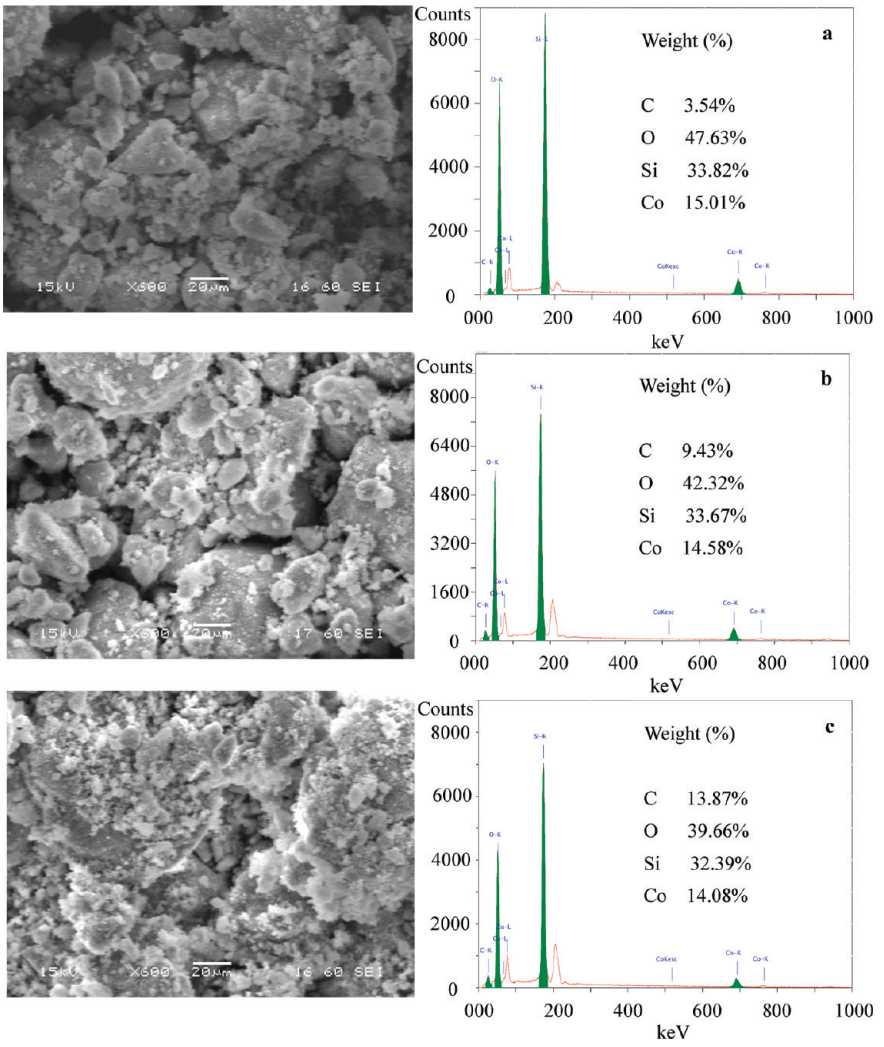

Figure 6. SEM-EDS analysis of the as-burnt catalysts (a) $C_{0.5}$, (b) C_1, and (c) $C_{1.5}$.

sustaining heat releasing process in air. A broad exothermic peak from 510 to 600 K was presented in the DTA curves, as compared in Figure 7c2−7e2. There was almost no exothermic peak from 510 to 600 K in Figure 7b2 for the as-burnt catalyst $C_{0.5}$. This result was in accordance with the Raman spectrum and EDS analysis that little amorphous carbon left in the as-burnt catalyst $C_{0.5}$. It was compared in Figure 7b1−7e1 that with increase of the initial content of CA in the precursors, the weight loss which was assigned to the oxidation of amorphous carbon increased gradually. Spontaneously, the area of the exothermic peak from about 510 to 600 K increased gradually. The DTA cure of the as-burnt catalyst $C_{1.5}$ displayed a much sharper exothermic peak than others. It was notable that about 11.5% weight loss which arose from amorphous carbon oxidation was displayed in Figure 7e1 for the as-burnt catalyst $C_{1.5}$ with M/CA = 1/1.5, much larger than 4.0% weight loss of the as-burnt catalyst C_1 with M/CA = 1/1. It was deduced that much excessive amorphous carbon which was derived from the pyrolysis of the residue organics was left in the as-burnt catalysts $C_{1.5}$.

3.7. TPR Analysis of the As-Burnt Catalysts without Reduction. TPR profiles of the calcined catalyst C_N before reduction prepared by the conventional impregnation method as well as the as-burnt catalysts prepared by the surface impregnation combustion method are compared in Figure 8. In agreement with previous reports,[10,11] the TPR peaks for the calcined catalyst C_N from 520 to 680 K were attributed to the two steps reduction of Co_3O_4 ($Co_3O_4 \rightarrow CoO \rightarrow CoO$). For the as-burnt catalysts $C_{0.7}$, C_1, and $C_{1.5}$, a low temperature TPR peak at about 490 K is compared in Figure 8c−8e. The similar experimental phenomena to that low-temperature TPR peak at about 473 K for the calcined Co-based catalyst was exhibited in many literatures.[19,34−39] Most of them[19,34−38] gave the explanation that this low-temperature TPR peak might be assigned to the decomposition of residual nitrate species. It was compared in Figure 8; the TCD signal in terms of hydrogen consumption at about 490 K which was attributed to the decomposition of residual nitrate species increased at first and reached a maximum for the as-burnt catalysts C_1 with M/CA = 1/1, and then decreased furthermore. As the combustion process was considered as a redox process and CA acted as reductant, with low content of CA (reductant) in the precursor of the as-burnt catalyst $C_{0.5}$, the combustion process was the most severe (as compared in Figure 1b), and the decomposition of residual nitrate species proceeded more deeply. Therefore, there was no TPR peak at about 490 K in Figure 8a. With increase of the content of CA, the combustion process was much gentler and the flame temperature was lower, so more residual nitrate species were left in the as-burnt

dx.doi.org/10.1021/cs200294d |ACS Catal. 2011, 1, 1225–1233

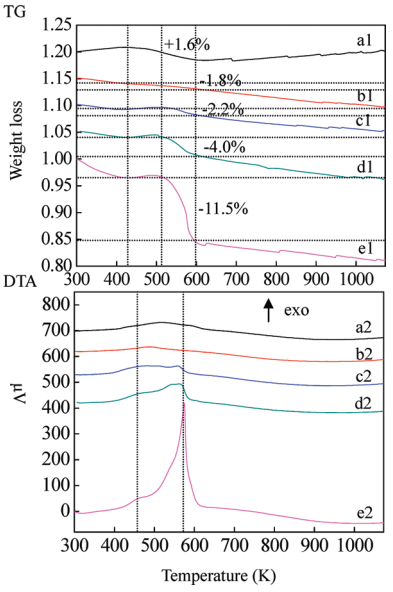

Figure 7. TG curves of (a1) C_N, (b1) $C_{0.5}$, (c1) $C_{0.7}$, (d1) C_1, and (e1) $C_{1.5}$, as well as the DTA curves of (a2) C_N, (b2) $C_{0.5}$, (c2) $C_{0.7}$, (d2) C_1, and (e2) $C_{1.5}$.

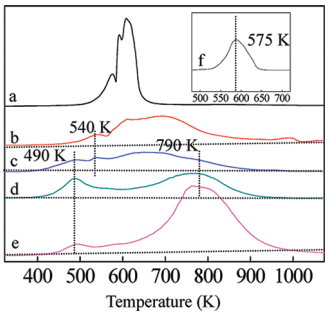

Figure 8. TPR profiles of (a) the calcined catalyst C_N as well as the as-burnt catalysts (b) $C_{0.5}$, (c) $C_{0.7}$, (d) C_1, (e) $C_{1.5}$, and (f) CuO.

catalysts. But for the as-burnt catalyst $C_{1.5}$ with M/CA = 1/1.5, more ammonia was used to adjust the pH value. The majority of nitrate iron was in the form of NH_4NO_3 which was proved by XRD analysis of the precursor, and the decomposition of NH_4NO_3 happened before the autocombustion. As a result, a small amount of residual nitrate species were left in the as-burnt catalyst $C_{1.5}$.

As displayed in Figure 8b−8d, a broad diffuse peak located from about 500 to 750 K was assigned to the reduction of CoO phase to metallic Co, much higher than that of the calcined catalyst C_N. The diffuse peaks indicated the existence of several species reduced at approximately the same temperature. It was generally considered that a smaller Co crystalline size needs a higher reduction temperature.[10,11,40,41] This proved that a part of CoO left in the as-burnt catalysts had smaller Co crystalline size and was hard to be reduced. The TPR profiles in this region (500−750 K) were not legible enough because the majority of Co-based phase in the as-burnt catalysts was already reduced by H_2 and CH_4 during the combustion process when using this novel surface impregnation combustion method. It was compared in Figure 8b−8e; the TPR profiles in the region from 500 to 750 K gradually changed from a broad diffuse peak to a flat line with continually increase of the content of CA, suggesting that the reduction degree of the as-burnt catalysts increased with the increased initial content of CA in the precursors.

As compared in Figure 8c−8e, a broad peak at about 790 K might be assigned to the hydrogenation of amorphous carbon. As the TPR profiles of some carbon supported metal catalysts had the similar broad peak at about 800 K,[42−44] and TPR-MS was used to identify the formation of methane.[44] With increase of the content of CA, the area of the broad peak at about 790 K increased, indicating that more amorphous carbon was left in the as-burnt catalysts. These results were in accordance with those of Raman spectrum, EDS analysis, and the TD-DTA measurement in air. It was worth emphasizing that the area of the broad TPR peak at about 790 K of $C_{1.5}$ in Figure 8e was much larger than others, and the amount of amorphous carbon left in the as-burnt catalyst $C_{1.5}$ measured by TPR was highly in accord with that measured by TG analysis in the air atmosphere.

The reduction degree of catalyst C_N was evaluated according to the hydrogen amount consumed from 303 to 723 K. As shown in Figure 8f, CuO was used to calibrate the TCD signal for H_2 consumption.[18,19] For the as-burnt catalysts, the reduction degree was calculated by the percentage of the difference value to the theoretical amount of hydrogen consumed, and the difference value was the theoretical amount of hydrogen consumed minus the actual amount of hydrogen consumed which was measured by TPR profiles, and the actual uptake of hydrogen in TPR profiles was that the unreduced CoO phase in the as-burnt catalysts consumed. As compared in Table 1, the reduction degree of the as-burnt catalyst increased with increase of the content of CA. For the as-burnt catalyst $C_{0.5}$ with M/CA = 1/0.5, the reduction degree was only 31%; however, the reduction degree was up to 95% for the as-burnt catalyst $C_{1.5}$ with M/CA = 1/1.5. It proved that the state of Co phase in the as-burnt catalyst $C_{1.5}$ was almost reduced to metallic Co supported on SiO_2 when using this novel surface impregnation combustion method.

3.8. Hydrogen Chemisorption. Chemisorption of hydrogen on the catalyst C_N which was after 10 h of reduction by 100% H_2 and passivated by 1% O_2 in argon, as well as the as-burnt catalysts without further reduction, are compared in Table 1. Uptakes of hydrogen on the support and amorphous carbon were negligible. The total H_2 uptake by catalysts followed the order $C_{1.5} > C_1 > C_{0.7} > C_N$. On the basis of the reduction degree of the catalysts measured by TPR, the dispersion of catalysts was calculated. With increase of the initial content of CA in the precursors, the dispersion of the as-burnt catalysts increased gradually. As shown in Table 1, the cobalt particle sizes derived from H_2-chemisorption are in good accord with those calculated by XRD.

3.9. TEM Images of the As-Burnt Catalysts. Figure 9 displayed the TEM images of the calcined catalyst C_N, the as-burnt catalyst C_1 and $C_{1.5}$, respectively. It was compared in Figure 9b−9c, the particle-size distributions of the as-burnt catalysts were rather narrow with standard deviations at most 20% of the average size. The average size of the cobalt crystalline calculated from cobalt size distribution was compared in Table 1. It was clear that the average size of the cobalt crystalline obeyed the series: $C_N > C_{0.5} > C_{0.7} > C_1 > C_{1.5}$, which is in accord with the results of XRD and H_2-chemisorption in Table 1.

3.10. Activity of the Catalysts. The Brunauer−Emmett−Teller (BET) surface area and catalytic performance of C_N and the as-burnt catalysts for FTS were compared in Table 2. The BET surface area of silica (Q-50) was 57 $m^2\ g^{-1}$, whereas that of the as-burnt $C_{0.5}$ was 47.8 $m^2\ g^{-1}$. The decrease of the BET surface area was mainly derived from the disappearance or collapse of the pores of SiO_2.

dx.doi.org/10.1021/cs200294d |ACS Catal. 2011, 1, 1225–1233

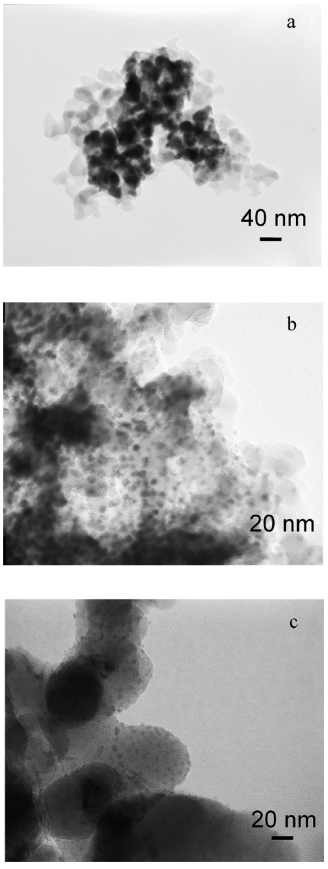

Figure 9. TEM images of (a) C_N, as-burnt catalysts (b) C_1 and (c) $C_{1.5}$.

In the preparation process of the as-burnt catalyst $C_{0.5}$, the combustion process was the fiercest, which was proved by TG-DTA curves in Figure 1b. Higher temperature made the SiO_2 pores collapse and increased the CoO crystalline size. With increase of the content of CA, the BET surface area of the as-burnt catalyst increased at first, and reached a maximum for the as-burnt catalysts C_1 with M/CA = 1/1, and then decreased. Because of increase of the content of CA, there were more gases liberated out which led to the porous structure, but the excessive CA resulted in oversupply of the carbonic residues, where the latter coated on the as-burnt catalysts and caused the decrease of the surface areas. The variation trend of the BET surface areas of the as-burnt catalysts was similar with that of Co crystalline change except the as-burnt $C_{1.5}$, as the BET surface areas were also influenced by the amount of the carbonic residues. Increasing the initial content of the CA in the precursors, more carbonic residues were left in the as-burnt catalysts, which lowered the BET surface areas of the as-burnt catalysts. But for the as-burnt catalyst $C_{0.5}$ during the combustion process, not much gas was emitted, and its BET surface area was very low because the porous structure was difficult to form. Consequently, the relationship among the CA content, catalyst surface area, and resultant Co crystalline size must be tuned finely. For the as-burnt catalyst $C_{1.5}$, from its smallest supported Co crystalline size, its surface area should be the largest. Because of the accumulation of excessive carbonic residues, its surface area was limited to 76.3 $m^2\ g^{-1}$. It was considered that for the as-burnt catalyst $C_{1.5}$, a part of the 4.0 nm Co particle was embeded in the bulky carbonic phase.

On the catalytic performances of these FTS catalysts as listed in Table 2, it is clear that the C_N catalyst exhibited limited CO conversion as low as 16.7%, mainly determined by its largest cobalt crystalline size and lower cobalt dispersion. Among all the as-burnt catalysts, only $C_{0.5}$ had no activity because it was almost unreduced as demonstrated in Figure 2 and Table 1. Being varied from $C_{0.7}$ to $C_{1.5}$, the supported cobalt crystalline size decreased, the reduction degree as well as cobalt dispersion of the as-burnt catalysts increased, and CO conversion generally increased. Higher reduction degree and higher dispersion were the main reason why the as-burnt catalysts exhibited higher activity than C_N. But for the as-burnt catalyst $C_{1.5}$ with M/CA = 1/1.5, the CO conversion was a little lower than the as-burnt catalyst C_1 with M/CA = 1/1. As one reason, more content of carbonic residues left in the as-burnt catalyst $C_{1.5}$, indicating that when using the same weight of the as-burnt catalysts, the as-burnt catalyst $C_{1.5}$ contained less weight of cobalt than C_1. As another reason, it was considered that a lot of carbonic residues accumulated on the surface of the as-burnt catalyst $C_{1.5}$, making the diffusion of syngas difficult and consequently lowering its apparent CO conversion, even with the smallest cobalt crystalline existing.

Table 2. Catalytic Performance of C_N and the As-Burnt Catalysts for FTS[a]

			Sel. (%)		
catalyst	BET[b] (m^2/g)	CO conversion (%)	CH_4	CO_2	α
C_N[c]	65.5	16.7	11.6	1.3	0.80
$C_{0.5}$	47.8	0	0	0	
$C_{0.7}$	78.9	31.3	13.8	2.8	0.78
C_1	85.0	47.2	21.2	3.7	0.73
$C_{1.5}$	76.3	42.3	42.3	3.9	0.56

[a] Reaction conditions: T = 513 K, P = 1.0 MPa, catalyst weight: 1 g, Co loading: 15 wt %, n-hexadecane: 20 mL, stirring speed: 2000 rpm, reaction time: 4 h, syngas: CO/H_2 = 1/2, W/F (CO + H_2 + Ar) = 10 g h mol^{-1}. [b] Determined by N_2 physical desorption at 77 K. [c] Conventional impregnation catalyst reduced at 723 K for 10 h in H_2.

For the as-burnt catalyst $C_{1.5}$, methane selectivity was high. One reason was its smallest cobalt crystalline, as finely dispersed metallic crystalline was not suitable for carbon chain growth process but methane formation was promoted here. Another reason was the diffusion process of syngas to reach the cobalt crystallines embedded by carbonic residues. H_2 diffused more quickly than CO inside micropores of these carbonic residues, leading to the very higher H_2/CO ratio than the original ratio at the cobalt surface, resulting in excessive methane.

In general, the as-burnt catalyst which was prepared by this novel surface impregnation autocombustion method obviously promoted the catalytic activity if compared with the C_N catalyst prepared by the conventional impregnation method which was reduced at 723 K for 10 h in hydrogen. Comparing with the catalytic performance of C_N in Table 2 and the former data,[45−47] the CO conversion of the as-burnt catalyst C_1 was almost 3-fold of that of the catalyst C_N prepared by the conventional incipient-wetness impregnation method, but the CH_4 selectivity was a little higher which might be derived from the smaller Co crystalline size and Co particles embedded in carbonic residues.

4. CONCLUSION

A series of the as-burnt metallic catalysts (Co/SiO_2) were prepared by a novel surface impregnation autocombustion method using cobalt nitrates and CA, and burnt in the argon atmosphere.

dx.doi.org/10.1021/cs200294d |ACS Catal. 2011, 1, 1225–1233

Supported nanostructured metallic Co/SiO_2 catalysts which were prepared without further reduction were used directly in slurry phase Ficher−Tropsch synthesis. During the combustion process, H_2 and CH_4 which came from the decomposition of the CA were the reducing agents for synthesizing metallic Co from Co^{2+} in the chelated compounds. With increase of the initial content of CA in the precursors, the reduction degree and the cobalt dispersion of the as-burnt catalysts increased gradually, as well as the cobalt crystalline size gradually decreased, but more carbonic residues were left in the as-burnt catalysts with continual increase of the content of CA. Comparing with the catalyst C_N which was prepared by the conventional impregnation method and reduced at 723 K for 10 h in pure hydrogen, the CO conversion of the as-burnt catalyst C_1 with M/CA = 1/1 was almost 3-fold of that of the catalyst C_N.

The sol−gel autocombustion method described herein provided a convenient way to prepare supported nanostructured metallic catalysts. This surface impregnation autocombustion method may open a new way to prepare metallic catalysts without further reduction, especially the catalysts which were difficult to be reduced at higher temperature.

■ ASSOCIATED CONTENT

Supporting Information. Figure of the XRD patterns of the as-burnt catalysts $C_{1.5}$ calcined at 1023 K for 3 h. This material is available free of charge via the Internet at http://pubs.acs.org.

■ AUTHOR INFORMATION

Corresponding Author

*Phone: +(81)-76-445-6846. Fax: +(81)-76-445-6846. E-mail: tsubaki@eng.u-toyama.ac.jp.

■ REFERENCES

(1) Deutschmann, O.; Knözinger, H.; Kochloefl, K.; Turek, T. *Heterogeneous Catalysis and Solid Catalysts*; Wiley-VCH: Weinheim, Germany, 2009; pp 38−39.
(2) Deutschmann, O.; Knözinger, H.; Kochloefl, K.; Turek, T. *Heterogeneous Catalysis and Solid Catalysts*; Wiley-VCH: Weinheim, Germany, 2009; pp 82−93.
(3) Li, Y. M.; Somorjai, G. A. *Nano Lett.* **2010**, *10*, 2289–2295.
(4) Farmer, J. A.; Campbell, C. T. *Science* **2010**, *329*, 933–936.
(5) Yin, Y. D. *Nano Res.* **2011**, *4*, 1–2.
(6) Khodakov, A. Y.; Chu, W.; Fongarland, P. *Chem. Rev.* **2007**, *107*, 1692–1744.
(7) Iglesia, E. *Appl. Catal.* **1997**, *161*, 59–78.
(8) Iglesia, E.; Soled, S. L.; Fiato, R. A.; Via, G. H. *J. Catal.* **1993**, *143*, 345–368.
(9) Ali, S.; Chen, B.; Goodwin, J. G. *J. Catal.* **1995**, *157*, 35–41.
(10) Sun, S. L.; Tsubaki, N.; Fujimoto, K. *Appl. Catal., A* **2000**, *202*, 121–131.
(11) Tsubaki, N.; Sun, S. L.; Fujimoto, K. *J. Catal.* **2001**, *199*, 236–246.
(12) Prieto, G.; Martínez, A.; Concepción, P.; Tost, R. M. *J. Catal.* **2009**, *266*, 129–144.
(13) Martínez, A.; López, C.; Márquez, F.; Díaz, I. *J. Catal.* **2003**, *220*, 486–499.
(14) Zhang, Q. H.; Kang, J. C.; Wang, Y. *ChemCatChem* **2010**, *2*, 1030–1058.
(15) Chu, W.; Wang, L. N.; Chernavskii, P. A.; Khodakov, A. Y. *Angew. Chem., Int. Ed.* **2008**, *47*, 5052–5055.
(16) Sietsma, J. R. A.; Meeldijk, J. D.; Breejen, J. P. D.; Helder, M. V.; Dillen, A. J. V.; Jongh, P. E. D.; Jong, K. P. D. *Angew. Chem., Int. Ed.* **2007**, *46*, 4547–4549.
(17) Jiang, Y. W.; Yang, S. G.; Hua, Z. H.; Huang, H. B. *Angew. Chem., Int. Ed.* **2009**, *48*, 1–4.
(18) Yung, M. M.; Holmgreen, E. M.; Ozkan, U. S. *J. Catal.* **2007**, *247*, 356–367.
(19) Martínez, A.; Prieto, G.; Rollán, J. *J. Catal.* **2009**, *263*, 292–305.
(20) Zowtiak, J. M.; Bartholomew, C. H. *J. Catal.* **1983**, *83*, 107–120.
(21) Reuel, R. C.; Bartholomew, C. H. *J. Catal.* **1984**, *85*, 63–77.
(22) Pathak, L. C.; Singh, T. B.; Das, S.; Verma, A. K.; Ramachandrarao, P. *Mater. Lett.* **2002**, *57*, 380–385.
(23) Huang, J. G.; Zhuang, H. R.; Li, W. L. *Mater. Res. Bull.* **2003**, *38*, 149–159.
(24) Chandradass, J.; Kim, K. H. *Adv. Powder Technol.* **2010**, *21*, 100–105.
(25) Wei, Z. X.; Wei, L.; Gong, L.; Wang, Y.; Hu, C. W. *J. Hazard. Mater.* **2010**, *177*, 554–559.
(26) Li, Y. Y.; Xue, L. H.; Fan, L. F.; Yan, Y. W. *J. Alloy. Compd.* **2009**, *478*, 493–497.
(27) Li, W. D.; Li, J. Z.; Guo, J. K. *J. Eur. Ceram. Soc.* **2003**, *23*, 2289–2295.
(28) Yang, R. Q.; Fu, Y. L.; Zhang, Y.; Tsubaki, N. *J. Catal.* **2004**, *228*, 23–35.
(29) Srivastava, R.; Srinivas, D.; Ratnasamy, P. *J. Catal.* **2005**, *233*, 1–15.
(30) Kwok, K. H.; Chiu, W. K. S. *Carbon* **2003**, *41*, 673–680.
(31) Ritter, U.; Scharff, P.; Siegmund, C.; Dmytrenko, O. P.; Kulish, N. P.; Prylutskyy, Y. I.; Belyi, N. M.; Gubanov, V. A.; Komarova, L. I.; Lizunova, S. V.; Poroshin, V. G.; Shlapatskaya, V. V.; Bernas, H. *Carbon* **2006**, *44*, 2694–2700.
(32) Wang, Z. H.; Choi, C. J.; Kim, B. K.; Kim, J. C.; Zhang, Z. D. *Carbon* **2003**, *41*, 1751–1758.
(33) Schwickardi, M.; Johann, T.; Schmidt, W.; Schüth, F. *Chem. Mater.* **2002**, *14*, 3913–3919.
(34) Sewell, G. S.; van Steen, E.; O'Connor, C. T. *Catal. Lett.* **1996**, *37*, 255–260.
(35) Sirijaruphan, A.; Horváth, A.; Goodwin, J. G., Jr.; Oukaci, R. *Catal. Lett.* **2003**, *91*, 89–94.
(36) Hong, J. P.; Chernavskii, P. A.; Khodakov, A. Y.; Chu, W. *Catal. Today* **2009**, *140*, 135–141.
(37) Ming, H.; Baker, B. G.; Jasieniak, M. *Appl. Catal., A* **2010**, *381*, 216–225.
(38) Hong, J. P.; Chu, W.; Chernavskii, P. A.; Khodakov, A. Y. *Appl. Catal., A* **2010**, *382*, 28–35.
(39) Hong, J. P.; Chu, W.; Chernavskii, P. A.; Khodakov, A. Y. *J. Catal.* **2010**, *273*, 9–17.
(40) Borg, Ø.; Eri, S.; Blekkan, E. A.; Storsæter, S.; Wigum, H.; Rytter, E.; Holmen, A. *J. Catal.* **2007**, *248*, 89–100.
(41) Prieto, G.; Martínez, A.; Concepción, P.; Moreno-Tost, R. *J. Catal.* **2009**, *266*, 129–144.
(42) Guerrero-Ruiz, A.; Sepúlveda-Escribano, A. A.; Rodríguez-Ramos, I. *Appl. Catal., A* **1994**, *120*, 71–83.
(43) Liang, C. H.; Ma, W. P.; Feng, Z. C.; Li, C. *Carbon* **2003**, *41*, 1833–1839.
(44) Jiao, G. P.; Ding, Y. J.; Zhu, H. J.; Li, X. M.; Li, J. W.; Lin, R. H.; Dong, W. D.; Gong, L. F.; Pei, Y. P.; Lu, Y. *Appl. Catal., A* **2009**, *364*, 137–142.
(45) Zhang, Y.; Yoneyama, Y.; Tsubaki, N. *Chem. Commun.* **2002**, *11*, 1216–1217.
(46) Zhang, Y.; Shinoda, M.; Tsubaki, N. *Catal. Today* **2004**, *93−95*, 55–63.
(47) Zhang, Y.; Koike, M.; Yang, R. Q.; Hinchiranan, S.; Vitidsant, T.; Tsubaki, N. *Appl. Catal.* **2005**, *292*, 252–258.